Exchange-biasing mechanism in $La_{2/3}Ca_{1/3}MnO_3/La_{1/3}Ca_{2/3}MnO_3$ multilayers

I. Panagiotopoulos
Institute of Materials Science, National Centre for Scientific Research, ''Demokritos,'' 153 10 Aghia Paraskevi, Athens, Greece

C. Christides
Department of Engineering Sciences, School of Engineering, University of Patras, 26110 Patras, Greece

M. Pissas and D. Niarchos
Institute of Materials Science, National Centre for Scientific Research, ''Demokritos,'' 153 10 Aghia Paraskevi, Athens, Greece
(Received 13 November 1998)

A series of $[La_{2/3}Ca_{1/3}MnO_3(\Lambda/2)/La_{1/3}Ca_{2/3}MnO_3(\Lambda/2)]_{15}$ multilayers, with bilayer thicknesses Λ between 2 and 32 nm, has been prepared by pulsed laser deposition. The study of their magnetic and magnetotransport properties reveals the presence of an exchange-biasing mechanism at low temperatures. Zero-field-cooling and field-cooling magnetic measurements reveal a blocking temperature around 70 K that is independent from the bilayer thickness, whereas the average film magnetization becomes zero at 250 K. It is observed that the exchange-biasing field H_{EB} at 10 K follows the variation of coercive field H_c with Λ, indicating that there is a significant contribution in H_c from the exchange anisotropy at the interfaces. The optimum exchange-biasing properties were observed in multilayers with $\Lambda = 8$ nm. [S0163-1829(99)04525-7]

I. INTRODUCTION

The existence of unidirectional anisotropy due to exchange coupling between a ferromagnetic and an antiferromagnetic phase was first reported in oxide-coated fine particles[1] of Co. Characteristically, exchange anisotropy results in a displaced magnetic hysteresis loop when the sample is field cooled through the Neel temperature of the antiferromagnetic phase. In early studies, this loop displacement has been explained by assuming an ideal ferromagnetic/antiferromagnetic interface with uncompensated moments in the atomic plane of the antiferromagnetic layer at the ferromagnetic (FM)/ antiferromagnetic (AF) boundary.[1] Up to date exchange anisotropy effects have been studied mainly in AF/FM systems consisting of transition-metal alloys and metallic oxides (e.g., ferromagnetic=Co, NiFe, Fe_3O_4, and antiferromagnetic=CoO, FeMn),[1–8] where the ferromagnetic or antiferromagnetic interactions are due to *direct exchange* coupling.

Besides the scientific interest to investigate the elusive mechanism of ferromagnetic/antiferromagnetic coupling, a great deal of attention has recently been focused on the technological applications of the resultant exchange bias in spin-valve magnetic field sensors and nonvolatile memories for magnetic storage devices.[9] Also, a large amount of work has been generated in order to evaluate the applicability of Lanthanum manganites, presenting the colossal magnetoresistance (CMR) effect, in spin-polarized tunnel junctions[10] as well as in spin-polarized current injection devices.[11] Fabrication of these heterostructures involves contact of the conducting $La_{2/3}Sr_{1/3}MnO_3$ oxides with another perovskite material. Since the $La_{2/3}R_{1/3}MnO_3$ (R=Sr, Ca) layers are FM their contact with AF perovskite layers may give rise to exchange coupling and, subsequently, in exchange-biasing effects at the ferromagnetic/antiferromagnetic interfaces that may alter the magnetotransport properties of the junctions. To the best of our knowledge, a systematic study about the presence of exchange coupling in CMR layers has not yet been reported.

In this study, our aim is to develop an exchange-biasing mechanism in a series of manganese perovskite $[La_{1/3}Ca_{2/3}MnO_3/La_{2/3}Ca_{1/3}MnO_3]_{15}$ multilayers, consisting from alternating stacks of $La_{2/3}Ca_{1/3}MnO_3$ (FM) layers and $La_{1/3}Ca_{2/3}MnO_3$ (AF) layers[12–14] where the magnetic interactions cannot be described by direct exchange.[12–15] The structural compatibility of the selected AF and FM layers permits coherent growth of the superlattice that satisfy the conditions for magnetic coupling at the interfaces. A systematic study of the exchange field and coercivity is presented as a function of the bilayers thickness and the substrate used.

II. EXPERIMENTAL DETAILS

Thin films were prepared by pulsed laser deposition (PLD) of bulk stoichiometric $La_{2/3}Ca_{1/3}MnO_3$ (FM) and $La_{1/3}Ca_{2/3}MnO_3$ (AF) targets on (100) $LaAlO_3$ single-crystal substrates. The targets were prepared by standard solid-state reaction from La_2O_3, $CaCO_3$, and MnO_2 powders sintered at 1325 °C for 5 days with two intermediate grindings. The beam of an LPX105 eximer laser (Lambda Physic), operating with KrF gas ($\lambda = 248$ nm), was focused on a rotating target. In order to grow a multilayer structure, the AF and FM targets were mounted on a step-motor controlled rotatable carrier that allows different targets to be sequentially exposed in the beam path. The pulse energy was 225 mJ, resulting in a fluence of 1.5 J/cm^2 on the target. The substrate was located at a distance of 6 cm from the target, by the edge of the visible extent of the plume. During deposition the substrate temperature was stabilized at 700 °C and the oxygen pressure in the chamber was 0.3 Torr, resulting in a deposition rate of 0.04 nm per pulse.

A series of $[AF(\Lambda/2)/FM(\Lambda/2)]_{15}$ multilayers was de-

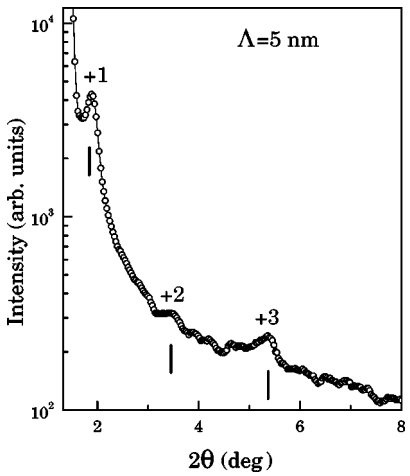

FIG. 1. A typical low-angle XRD pattern where the superlattice Bragg peaks from the $LaAlO_3$/AF(40 nm)/$[FM(\Lambda/2)/AF(\Lambda/2)]_{15}$ multilayer, with $\Lambda=5$ nm, are shown. The tick marks indicate the positions of the superlattice peaks with order $n=1$, 2, and 3 (from left to right).

posited on 40-nm-thick AF buffer layer, forming bilayers with superlattice periods $\Lambda=2$, 5, 8, 10, 20, and 32 nm. Also, for comparison we have prepared an $[AF(4\ nm)/FM(4\ nm)]_{15}$ multilayer on a (100) $SrTiO_3$ single-crystal substrate with 40-nm-thick AF buffer layer (named STO), and a similar sample on a (100) $LaAlO_3$ single-crystal substrate without buffer layer (named LAO). X-ray-diffraction (XRD) spectra were collected at ambient conditions with a Siemens D500 diffractometer using Cu-Kα radiation. Magnetic measurements were performed in a Quantum Design MPMSR2 superconducting quantum interference device (SQUID) magnetometer, with the field applied in the film plane. The magnetotransport measurements have been carried out with the standard four-point probe method, applying the magnetic field parallel to current flow direction.

III. RESULTS

A. X-ray diffraction

The existence of the superstructure has been confirmed from the presence of low-angle superlattice Bragg-peaks and multiple satellite peaks around the (001), (002), and (003) Bragg reflections of the constituents. A typical pattern is displayed in Fig. 1 where the low-angle Bragg peaks from the AF/FM multilayers with $\Lambda=5$ nm are shown. As it is expected for multilayers with equal layer thicknesses[16] the intensities from even-order, low-angle peaks are suppressed. In Fig. 2 the XRD profiles reveal strong texturing along the pseudocubic (001) direction of the perovskite unit cell (a_p lattice constant) for the films grown on STO and LAO with $\Lambda=8$ nm, either with or without 40-nm AF buffer layer for the latter. The (00l) STO and (00l) LAO Bragg peaks ($l=1$, 2, and 3) interfere with the asymmetric intensity of the satellite peaks nearby the fundamental (zeroth order) peaks of the multilayer, introducing uncertainties in the quantitative analysis of the XRD spectra. Asymmetric intensity of the satellite peaks has been reported in multilayers[16,17] in which a chemical and/or strained interfacial profile is assumed along the growth direction of the superlattice. Since for all the examined Λ values there are no traces of mixed (001) and (110) textures on LAO and STO substrates, cumulative roughness effects resulting to extra surface roughness and mosaic spread[18] with increasing Λ can be excluded. Evidently, due to slight differences in the average (overall) out-of-plane lattice spacing a_p, the $n=+1$—next to

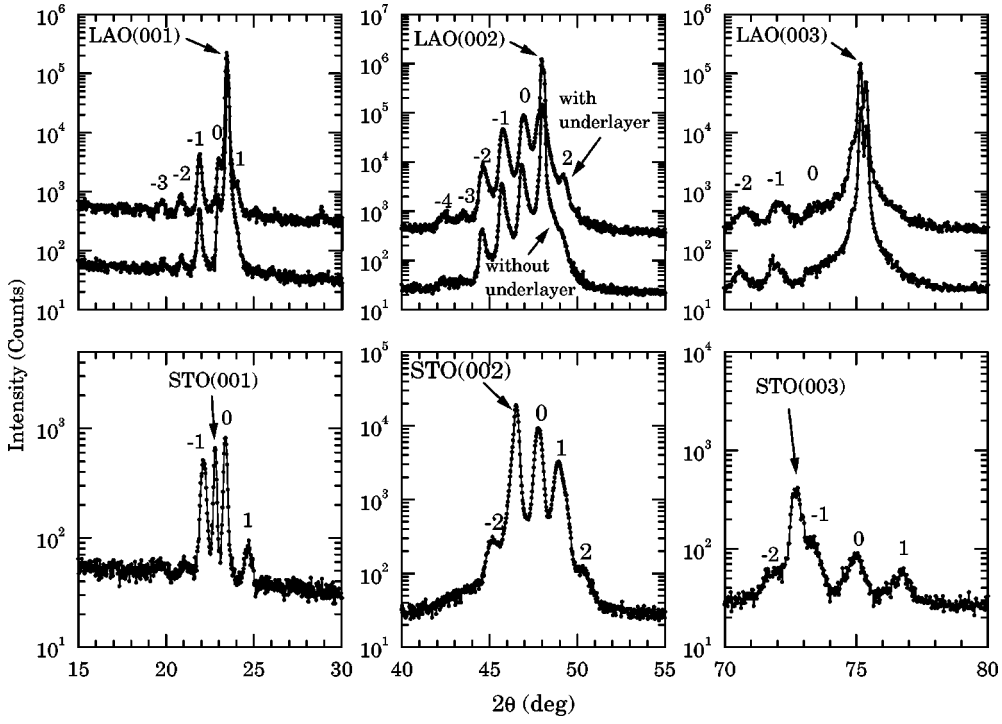

FIG. 2. XRD profiles of films with $\Lambda=8$ nm, grown on STO and LAO substrates, showing a strong preferred orientation along the pseudocubic (001) direction of the perovskite unit cell.

(001)LAO peak— and the $n=+2$—next to (002)LAO—satellite peaks are better resolved for the multilayer grown on the AF buffer layer than those observed for the film deposited directly on the LAO substrate.

Such variations of a_p were observed[19,20] in $La_{2/3}Ca_{1/3}MnO_3$ thin films grown on STO and LAO substrates, where the lattice distortions were found to be sensitive on deposition conditions (oxygen pressure, annealing), surface roughness of the substrate, and the film thickness. Our results reveal that a FM layer, 100-nm thick, on LAO exhibits an $a_p(\mathrm{FM})=0.394$ nm whereas its bulk value[21] is about 0.386 nm (with $a\approx c\approx a_p\sqrt{2}$, $b\approx 2a_p$ in the $Pnma$ space group), and a single AF layer exhibits an $a_p(\mathrm{AF})=0.381$ nm. The deviation of $a_p(\mathrm{FM})$ from its bulk value is comparable with that observed[22] in $La_{0.7}Ca_xMnO_3$ thin films with $x\approx 0.2$ ($a_p\approx 0.391$ nm). However, in Fig. 2 the position of the fundamental ($n=0$) peaks gives an average (overall) $a_p=0.3803$ nm for multilayers on top of STO, an $a_p=0.3874$ nm on LAO, and an $a_p=0.3864$ nm on AF buffer layer adjacent to LAO, suggesting a strain-driven mechanism for the deviations of the average lattice spacing in these multilayers.[23]

The lattice parameters of the substrate were estimated from the observed ($00l$) Bragg-peak positions (Fig. 2), where superposition with the diffracted intensity of the multilayer causes extra peak broadening and a small uncertainty in peak position. Since the estimated $a_p\approx 0.390$ nm of STO (expected 0.3905 nm) is greater than the $a_p\approx 0.379$ nm of LAO, the corresponding lattice mismatch between the, first deposited, AF layer and substrate will cause different layer modifications.[19,21] Using as a criterion the optimum CMR versus temparature performance (see next section), observed in these three films with $\Lambda=8$ nm, we decided to study systematically the variation of Λ in multilayers grown on LAO substrates with 40 nm of AF buffer layer. Figure 3 shows the XRD profiles as a function of Λ in the medium-angle range. The grouping of the satellite peaks indicates that for Λ up to 10 nm there is a coherent AF/FM superlattice, while for $\Lambda>10$ nm two uncoupled structures appear around the (002) Bragg peaks of the FM and AF lattice, respectively.

B. Magnetotransport properties in films grown on LAO and STO substrates

Magnetic hysteresis loops, measured at 10 K after cooling down from 300 K in zero-field cooled (ZFC) and 10 kOe in field cooled (FC), are shown in Fig. 4 for a $LaAlO_3/[\mathrm{FM}(4\ \mathrm{nm})/\mathrm{AF}(4\ \mathrm{nm})]_{15}$ film and a $SrTiO_3/\mathrm{AF}(40\ \mathrm{nm})[\mathrm{FM}(4\ \mathrm{nm})/\mathrm{AF}(4\ \mathrm{nm})]_{15}$ film. It is evident that the ZFC loop is symmetric around the zero field, while the FC loop is shifted towards negative fields. This effect can be attributed to exchange-biasing at the AF/FM interface, since single-layered FM films do not exhibit any loop displacement after the FC process. If H_1 is the lower and H_2 is the higher field value where the average film magnetization becomes zero, then the exchange-biasing field is defined as the loop shift $H_{EB}=-(H_1+H_2)/2$ and the coercivity as the half-width of the loop $H_c=(H_1-H_2)/2$. Thus for the FC loop on LAO we find an $H_{EB}=780$ Oe with $H_c=680$ Oe, and on STO an $H_{EB}=690$ Oe with $H_c=1000$ Oe. The larger

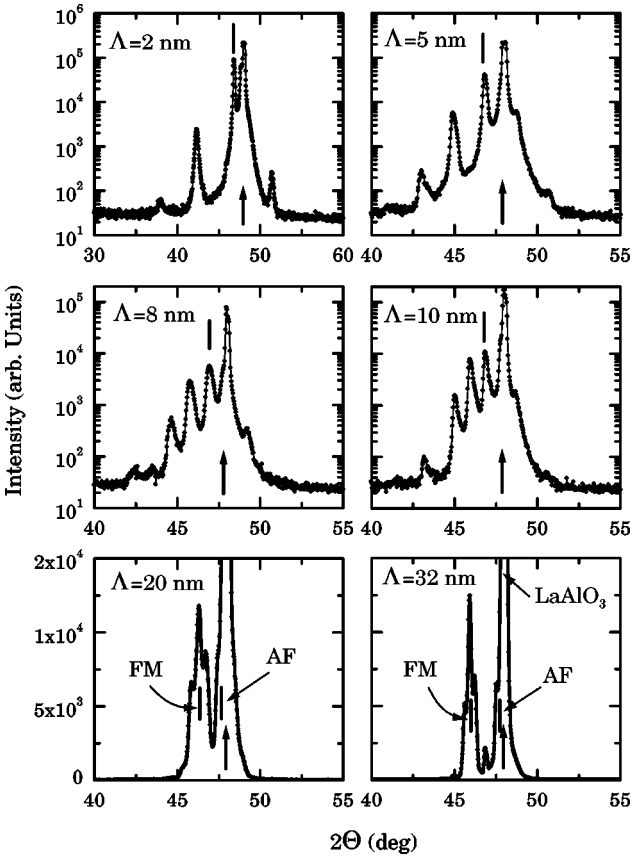

FIG. 3. XRD profiles plotted in the medium-angle range as a function of bilayer thickness Λ, for multilayers grown on LAO substrates with 40 nm of AF buffer layer. Note that for $\Lambda=2-10$ nm the intensity is in logarithmic scale while for $\Lambda=20$ and 32 nm we use the square-root intensity for clarity. Arrows indicate the (002) LAO peak and tick marks show the $n=0$ (fundamental) peak for $\Lambda<20$ nm, whereas for $\Lambda=20$ and 32 nm the ticks show peaks located at the (002) reflection of the FM and AF layer.

H_{EB} values of multilayers grown on LAO substrates, with or without buffer, justify our choice to study exchange-biasing effects in LAO films (see next section).

In Fig. 5 the variation of the normalized resistivity as a function of temperature, measured in 50 kOe (ρ_H) and in zero applied field (ρ_0) is shown. The resistivity increases drastically as we cool down from 300 K, spanning almost four orders of magnitude for the $LaAlO_3/[\mathrm{FM}(4\ \mathrm{nm})/\mathrm{AF}(4\ \mathrm{nm})]_{15}$ film whereas for the $SrTiO_3/\mathrm{AF}(40\ \mathrm{nm})\times[\mathrm{FM}(4\ \mathrm{nm})/\mathrm{AF}(4\ \mathrm{nm})]_{15}$ sample is less than an order of magnitude. The $\Delta\rho/\rho_H=[\rho_0-\rho_H]/\rho_H$ ratio gives an estimate of the collosal magnetoresistance (CMR) effect. This ratio becomes maximum at ~ 70 K for the multilayer film grown on LAO and at ~ 120 K for that on STO. Thus in both films the magnetotransport properties exhibit a number of different features relative to pure FM thin films.[20,22]

(i) The temperature variation of ρ_H, ρ_0, and the resultant CMR curve exhibit their maxima at temperatures well below the ordering temperature (T_c) of the FM layers. The presence of the insulating AF layers of $La_{1/3}Ca_{2/3}MnO_3$ within the multilayered structure may explain the steep increase of resistivity[24] below 150 K that changes the shape of the curves near the maxima. Also, the observed[20] magnetoresistive curves of 100-nm-thick $LAO(001)/La_{2/3}Ca_{1/3}MnO_3$

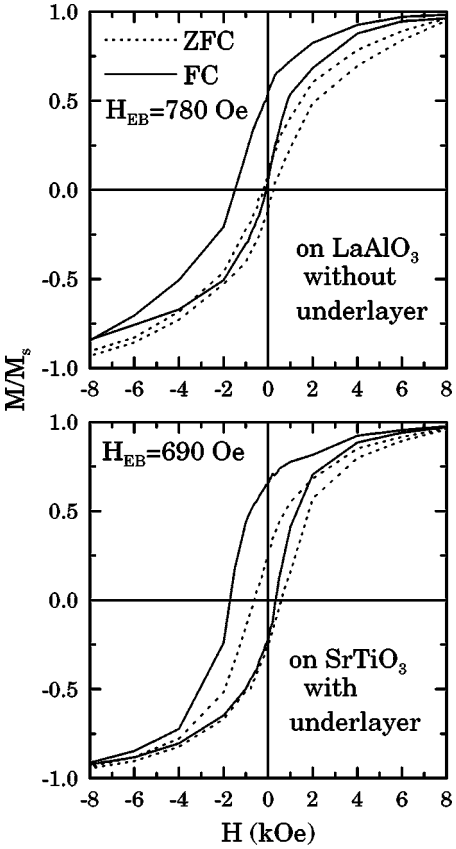

FIG. 4. Magnetic hysteresis loops, measured at 10 K after ZFC from 300 K and FC in 10 kOe, for a $LaAlO_3/[FM(4\ nm)/AF(4\ nm)]_{15}$ multilayer.

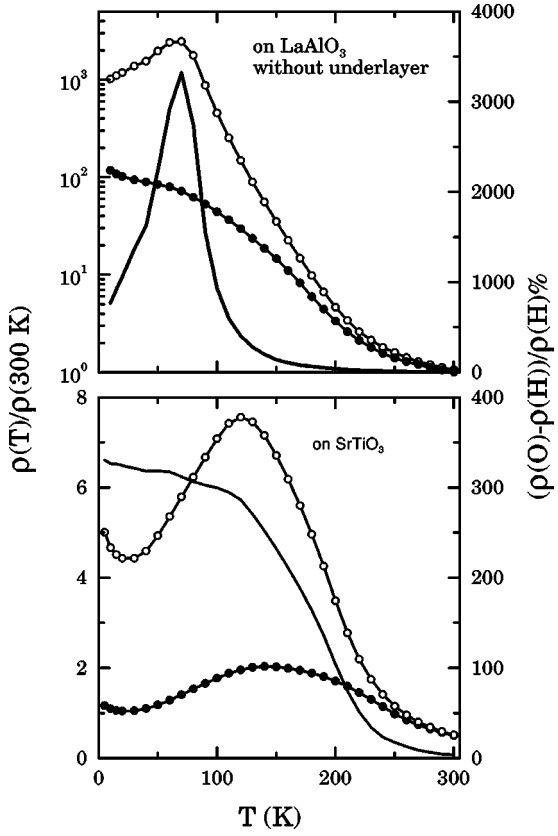

FIG. 5. Resistivity, normalized to the 300-K value, as a function of temperature, measured in 50 kOe (ρ_H) and in zero applied field (ρ_0) for a $[FM(4\ nm)/AF(4\ nm)]_{15}$ multilayer grown on $LaAlO_3$ and $SrTiO_3$ substrates. The CMR ratio $\Delta\rho/\rho_H=[\rho_0-\rho_H]/\rho_H$ is plotted as a solid line.

films, grown under the same deposition conditions, have shown that there are no significant grain boundary and/or low-crystallinity effects.[25–28] Thus in our case there is no experimental evidence indicating that the increased low-temperature resistivity in Fig. 5 originates from grain boundary effects.

(ii) The large differences (Fig. 5) observed in the CMR ratios between films grown on LAO and STO substrates show that the specific deposition conditions favor the enhancement of CMR on LAO. This can be attributed to strain relaxation inside the AF layers, since the AF film exhibits a pseudocubic lattice spacing ($a_p=0.381$ nm) comparable with that of (100) LAO ($a_p=0.379$ nm). Thus the lattice mismatch along the (100) LAO/AF direction is about 0.5% while in the (100)STO/AF interface is about 2.2%. Assuming similar surface roughness in both substrates, it is evident that the lower lattice mismatch favors pseudomorphic growth with less strain inside the deposited layers. For this reason we have prepared a series of multilayers, using an AF buffer layer between the LAO substrate and the multilayers.

C. Magnetotransport properties of multilayers grown on LAO substrates

In Fig. 6 magnetic hysteresis loops, measured at 10 K after ZFC and FC in 10 kOe, for a series of $LaAlO_3/AF(40\ nm)[FM(\Lambda/2)/AF(\Lambda/2)]_{15}$ multilayers are shown. It is evident that the FC loops exhibit a negative shift relative to the corresponding ZFC loops for all Λ. The estimated exchange biasing H_{EB} and coercive H_c fields are plotted in Fig. 7 as a function of Λ, defining an optimum composition for $\Lambda=8$ nm where the maximum in H_{EB} and H_c was observed. Thus we calculate for the FC loop an $H_{EB}=880$ Oe and an $H_c=800$ Oe which is almost double compared to the H_c value obtained from the ZFC loop for $\Lambda=8$ nm. Since exchange biasing is an interface related phenomenon a strong dependence on the individual FM and AF layer thicknesses is expected.[3] Accordingly, Fig. 7 shows that H_{EB} follows the variation of H_c with Λ, indicating that there is a significant contribution in H_c from the exchange anisotropy at the AF/FM interfaces.

Additional magnetic measurements were performed in order to investigate the origin of this effect. The temperature dependence of H_{EB} and H_c values is shown in Fig. 8 for $\Lambda=8$ nm. These values were estimated from isothermal loops measured in constant temperature intervals, after FC the sample from 300 K down to 10 K in 10 kOe and then warming up. It is evident that H_{EB} decreases and disappears around the so-called blocking temperature T_B about 70 K. The H_c values exhibit a similar trend, indicating a connection between the mechanisms that give rise to coercivity and loop displacement. The excess coercivity observed below T_B is induced by random exchange fields at the AF/FM interfaces. This low-temperature anisotropy can be treated as an additional energy barrier in the magnetic free energy, as in the case of superparamagnetic particles.[29] Thus by applying

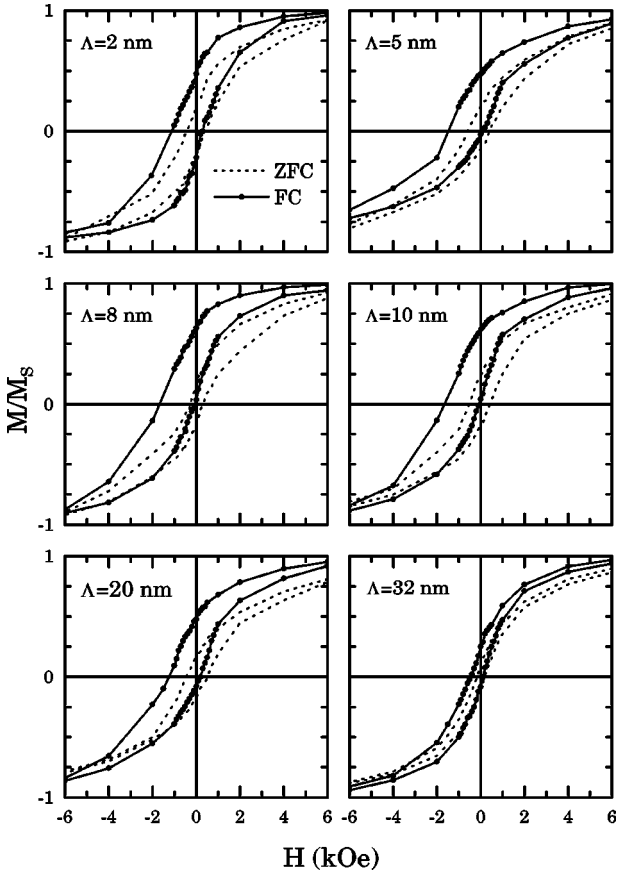

FIG. 6. Magnetic hysteresis loops, measured at 10 K after ZFC from 300 K and FC in 10 kOe, for a series of $LaAlO_3$/AF(40 nm)/$[FM(\Lambda/2)/AF(\Lambda/2)]_{15}$ multilayers.

the same model we derive an equation that describes the temperature variation of $H_c(T)$ with T:

$$H_c(T)=H_c(0)[1-(T/T_B)^{1/2}]+H_{back}, \qquad (3.1)$$

where $H_{back}(\approx 70$ Oe) takes into account the observed coercivity above the obtained T_B at 75 K. In Fig. 8 a good agreement between the experimental data (open circles) and the fitting curve (solid line) is observed. The existence of an H_{back} term can be explained from a recent magnetic phase diagram,[30] where it was shown that bulk $La_{1/3}Ca_{2/3}MnO_3$ undergoes a *charge ordering* transition[24] below 260 K,

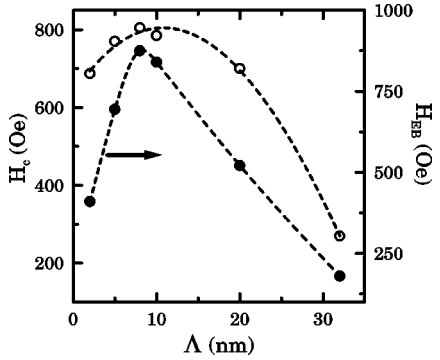

FIG. 7. Estimated H_{EB} (solid symbols) and H_c (open symbols) fields from FC isothermal loops at 10 K, for a series of $LaAlO_3$/AF(40 nm)/$[FM(\Lambda/2)/AF(\Lambda/2)]_{15}$ multilayers.

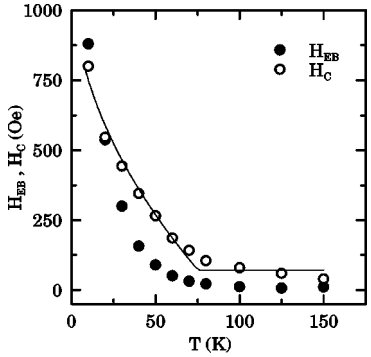

FIG. 8. Temperature dependence of H_{EB} (solid circles) and H_c (open circles) observed in $LaAlO_3$/AF(40 nm)/$[FM(4$ nm)/AF(4 nm)$]_{15}$ multilayer. The solid line presents a fitting curve according to Eq. (3.1).

whereas the long-range AF order sets in below 150 K. Thus above T_B a large H_{back} may arise from magnetic disorder at the AF/FM interfaces due to short-range magnetic interactions inside the $La_{1/3}Ca_{2/3}MnO_3$ layers that persist up to *charge ordering* transition of the multilayer. Accordingly, below T_B the enhancement of H_c is due to exchange anisotropy related to long-range AF interactions at the interfaces.

In Fig. 9 the ZFC and FC measurements of the magnetization, normalized to the total FM volume of the sample, are shown for different Λ as a function of temperature. Both measurements were performed by warming up in 1 kOe after having cooled in zero field and 10 kOe, respectively. The ZFC and FC curves coincide at temperatures higher than 100 K and become zero at about 250 K, where the Curie point T_C of the FM layers is expected. The ZFC curve exhibits a broad peak around the $T_B \sim 70$ K, whereas the FC curve ex-

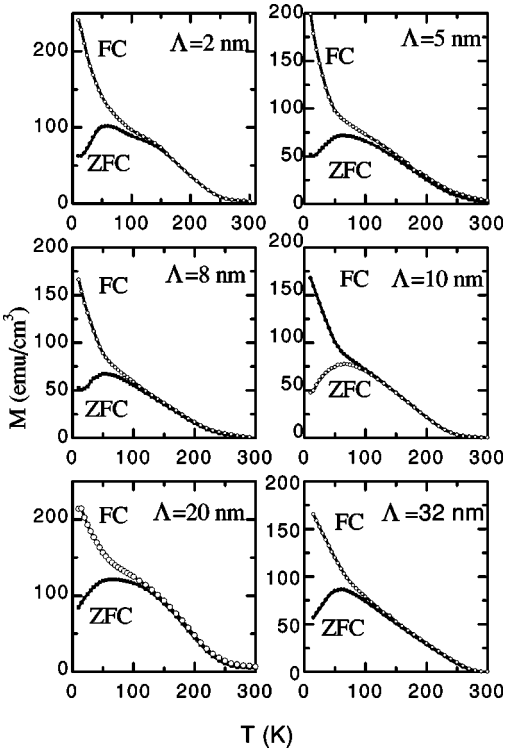

FIG. 9. ZFC and FC measurements of magnetization for a series of $LaAlO_3$/AF(40 nm)/$[FM(\Lambda/2)/AF(\Lambda/2)]_{15}$ multilayers.

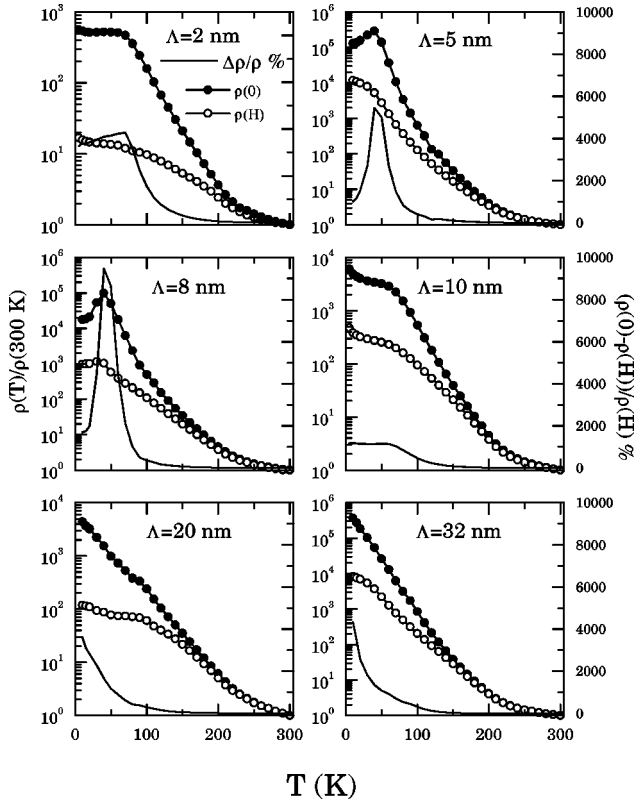

FIG. 10. Resistivity, normalized to the 300 K value, as a function of temperature, measured in 50 kOe (ρ_H) and in zero applied field (ρ_0) for a series of $LaAlO_3$/AF(40 nm)/$[FM(\Lambda/2)/AF(\Lambda/2)]_{15}$ multilayers. The CMR ratio $\Delta\rho/\rho_H=[\rho_0-\rho_H]/\rho_H$ is plotted as a solid line.

hibits a steep increase just below T_B. It is reasonable to assume that in the FC measurement an increase of magnetization results from the alignment of interfacial magnetic moments, giving rise to unidirectional anisotropy[5] below T_B. Hence, the observed hump below T_B in the ZFC curve can be attributed to thermally activated magnetic rotation over energy barriers caused by random exchange coupling at the AF/FM interfaces.

Figure 10 shows the variation of the normalized resistivity as a function of temperature, measured in 50 kOe (ρ_H) and in zero applied field (ρ_0). The resistivity increases drastically as we cool down from 300 K, spanning almost four orders of magnitude. Also, the CMR ratio becomes maximum in the temperature range below $T_B(\approx 70$ K). In Fig. 10 the steep increase of resistivity at low temperatures is in contrast with the decrease of ρ observed in epitaxial FM films.[20,22] This provides further experimental evidence that the insulating behavior[24] of the AF layer is dominant at low temperatures.

This extra contribution in ρ is different for every specimen and modifies the shape of the resultant CMR curves (Fig. 10). Clearly, the multilayers with $\Lambda=5$ and 8 nm exhibit a peak in the CMR response, indicating a special arrangement of spins at the AF/FM interfaces. As a consequence the characteristic CMR peak, that is usually reported nearby the ferromagnetic T_c of $La_{2/3}Ca_{1/3}MnO_3$ films,[12] is not observed in the ρ_0 versus temperature curve. This behavior is in agreement with the magnetothermal measurements (Fig. 9) where it is evident that the most drastic change of the average film magnetization does not occur near the T_c of the individual FM layers but at T_B. To answer why T_B remains more or less the same in the examined range of Λ values it is reasonable to consider that interfacial spin ordering is confined within a few atomic planes near the AF/FM interfaces, defining an *active* film volume V_{int}. Since T_B results from a thermally activated process, following an Arrhenius law,[29] its value depends on the active volume at the interfaces ($T_B \propto V_{int}$) which emerges to be similar in the examined multilayers.

IV. DISCUSSION AND CONCLUSIONS

Generally, the enhanced coercivity H_c observed[1–3] in exchange coupled FM/AF layers relative to the uncoupled FM layer is an unresolved theoretical issue. In exchange coupled AF/FM bilayers with $T_c < T_N$ (T_N being the Néel temperature of the AF layer) it was reported[31] that at low temperatures H_c varies as

$$H_c(T)=(A/t_{\mathrm{FM}}^{3/2}-BT/t_{\mathrm{FM}}^{2})/M_{\mathrm{FM}}, \tag{4.1}$$

where the factors A and B involve the exchange coupling strengths among the magnetic moments in the layers and at the interface and M_{FM} is the magnetization of the FM layer. According to Wu and Chien,[31] in exchange coupled FM/AF bilayers with $T_c \gg T_N$ only the $t_{\mathrm{FM}}^{-3/2}$ dependence of H_c [first term in Eq. (4.1)] can be experimentally established. Thus, in NiFe/CoO bilayers[31] ($T_c \gg T_N$) H_c decreases quasilinearly with increasing temperature up to T_N whereas H_{EB} exhibits a plateau at low temperatures and vanishes at T_N. In contrast, Fig. 8 shows that the observed behavior of H_c and H_{EB} with increasing temperature is different. The difference can be attributed to the complex mechanisms through which charge and spin ordering occurs in the $La_{1/3}Ca_{2/3}MnO_3$ layers.[24,30] In particular, the temperature dependence of the size of the magnetic domains inside the AF layers would be different for the super-exchange[24] coupled manganites. Since even in conventional exchange-bias multilayers there are many experimental aspects which have not been studied in detail,[32] further experimental studies are required to resolve such issues.

In summary, we have studied the variation of exchange biasing and coercive field as a function of Λ and temperature in $[La_{1/3}Ca_{2/3}MnO_3\ (\Lambda/2)/La_{2/3}Ca_{1/3}MnO_3\ (\Lambda/2)]_{15}$ multilayers grown by PLD on (100) $SrTiO_3$ and (100) $LaAlO_3$ single-crystal substrates. The maximum $H_{EB}=880$ Oe was observed for the sample with $\Lambda=8$ nm. The exchange-biasing mechanism sets in below a blocking temperature of 70 K and induces: (i) an enhacement of H_c in the FC hysteresis loops, and (ii) an increase of the CMR ratio.

ACKNOWLEDGMENT

The authors would like to thank N. Moutis for helping in the preparation of the target materials.

[1] W. H. Meiklejohn and C. P. Bean, Phys. Rev. **105**, 904 (1957); **102**, 1413 (1956).
[2] C. Tsang, N. Heiman, and K. Lee, J. Appl. Phys. **52**, 2471 (1981); **53**, 2605 (1982).
[3] R. Jungblut, R. Coehoorn, M. T. Johnson, J. van de Stegge, and A. Reinders, J. Appl. Phys. **75**, 6659 (1994).
[4] P. J. van der Zaag, A. R. Ball, L. F. Feiner, R. M. Wolf, and P. A. A. van er Heijden, J. Appl. Phys. **79**, 5103 (1996).
[5] K. Takano, R. H. Kodama, A. E. Berkowitz, W. Cao, and G. Thomas, Phys. Rev. Lett. **79**, 1130 (1997).
[6] T. Ambrose, R. L. Sommer, and C. L. Chien, Phys. Rev. B **56**, 83 (1997).
[7] Y. Ijiri, J. A. Borchers, R. W. Erwin, S. H. Lee, P. J. Van der Zaag, and R. M. Wolf, Phys. Rev. Lett. **80**, 608 (1998).
[8] J. Nogues, D. Lederman, T. J. Moran, I. Shuller, and K. V. Rao, Appl. Phys. Lett. **68**, 3186 (1998).
[9] G. A. Prinz, *in Ultrathin Magnetic Structures II*, edited by B. Heinrich and J. A. C. Bland (Springer-Verlag, Berlin, 1994), p. 36-42.
[10] Yu Lu, X. W. Li, G. Q. Gong, G. Xiao, A. Gupta, P. Lecoeur, J. Z. Sun, Y. Y. Wang, and V. P. Dravid, Phys. Rev. B **54**, 8357 (1996).
[11] V. A. Vasko, V. A. Larkin, P. A. Kraus, K. R. Nikolaev, D. E. Grupp, C. A. Nordman, and A. M. Goldman, Phys. Rev. Lett. **78**, 1134 (1997).
[12] P. Schiffer, A. P. Ramirez, W. Bao, and S.-W. Cheong, Phys. Rev. Lett. **75**, 3336 (1995).
[13] P. G. Radaelli, D. E. Cox, M. Marezio, S.-W. Cheong, P. E. Schiffer, and A. P. Ramirez, Phys. Rev. Lett. **75**, 4488 (1995).
[14] E. O. Wollan and W. C. Koehler, Phys. Rev. **100**, 545 (1955).
[15] C. Zener, Phys. Rev. **82**, 403 (1951); P. W. Anderson and H. Hasegawa, *ibid.* **100**, 675 (1955).
[16] E. E. Fullerton, I. K. Schuller, H. Vanderstraeten, and Y. Bruynseraede, Phys. Rev. B **45**, 9292 (1992).
[17] J. Mattson, R. Bhadra, J. B. Ketterson, M. Brodsky, and M. Grimsditch, J. Appl. Phys. **67**, 2873 (1990).
[18] R. A. Rao, D. Lavric, T. K. Nath, C. B. Eom, L. Wu, and F. Tsui, Appl. Phys. Lett. **73**, 3294 (1998).
[19] O. I. Lebedev, G. Van Tendeloo, S. Amelinckx, B. Leibold, and H. U. Habermeier, Phys. Rev. B **58**, 8065 (1998).
[20] I. Panagiotopoulos, G. Kallias, M. Pissas, V. Psycharis, and D. Niarchos, Mater. Sci. Eng., B **53**, 272 (1998).
[21] Q. Huang, A. Santoro, J. W. Lynn, R. W. Erwin, J. A. Borchers, J. L. Peng, K. Ghosh, and R. L. Greene, Phys. Rev. B **58**, 2684 (1998).
[22] S. V. Pietambaram, D. Kumar, R. K. Singh, and C. B. Lee, Phys. Rev. B **58**, 8182 (1998).
[23] T. Y. Koo, S. H. Park, K-B. Lee, and Y. H. Jeong, Appl. Phys. Lett. **71**, 977 (1997).
[24] M. T. Fernandez-Diaz, J. L. Martinez, J. M. Alonso, and E. Herrero, Phys. Rev. B **59**, 1277 (1999).
[25] E. S. Gillman, M. Li, and K.-H. Dahmen, J. Appl. Phys. **84**, 6217 (1998).
[26] C.-C. Chen and A. de Lozanne, Appl. Phys. Lett. **73**, 3950 (1998).
[27] C. Srinitiwarawong and M. Ziese, Appl. Phys. Lett. **73**, 1140 (1998).
[28] A. Gupta, G. Q. Gong, G. Xiao, P. R. Duncombe, P. Lecoeuer, P. Trouilloud, Y. Y. Wang, V. P. Dravid, and J. Z. Sun, Phys. Rev. B **54**, 15 629 (1996).
[29] B. D. Cullity, *Introduction to Magnetic Materials* (Addison-Wesley, Reading, MA, 1972), p. 413-418.
[30] A. J. Milllis, Nature (London) **392**, 147 (1998).
[31] X. W. Wu and C. L. Chien, Phys. Rev. Lett. **81**, 2795 (1998).
[32] J. Nogues and I. K. Schuller, J. Magn. Magn. Mater. **192**, 203 (1999).